PROCEEDINGS, 45rd Workshop on Geothermal Reservoir Engineering
Stanford University, Stanford, California, February 10-12, 2020
SGP-TR-213

Foot-scale Evaluation of CO_2-Responsive Polymer and CO_2 Binary Fluid as an Alternative Fracturing Fluid for Enhanced Geothermal Systems

Guoqing Jian,[1] Carlos A. Fernandez[1]*, Jeff Burghardt,[1] Alain Bonneville,[1]

Varun Gupta,[1] and Geoffrey Garrison[2]

[1]Pacific Northwest National Laboratory, Richland, WA 99352, United States

[2]Altarock Energy, Inc. Seattle, WA 98103

Carlos.Fernandez@pnnl.gov

Keywords: Enhanced Geothermal Systems, polyallylamine, CO_2-reponsive, stimulation

ABSTRACT

A foot-scale high-temperature true-triaxial fracturing apparatus was used to conduct hydraulic fracture tests on rock samples. The fracturing tests used different fluids including water, CO_2, CO_2 with water, and CO_2 with a 1% polyallylamine (PAA)/water solution. The tests were conducted with both constant pressure injection and constant flow rate injection modes. CO_2-based fracturing fluids were found to produce higher breakdown pressures, high transient flow rates, and produce higher-conductivity fractures as compared to water-based fracturing fluids. Additionally, faster pressurization rates with CO_2-based fracturing fluids (obtained when fracturing at constant flow rate mode) are found to be associated with higher fracture conductivities. When fracturing with CO_2-based fluids in the presence of a PAA aqueous solution, for example if the rock is saturated with 1wt% PAA in water, the volume expansion caused by CO_2-induced cross-linking of PAA leads to a faster pressure increase due to the associated volume expansion and increase in viscosity. It was also found that CO_2 as a fracturing fluid injected in hot dry rock (HDR) attain the highest fracture conductivity only when injected at very high flow rates, followed very closely by the CO_2/PAA fracturing fluid system that generates fractures with, on average, similarly high conductivity values though independently of injection flow rate and using 1/6 of the mass of CO_2 as compared to CO_2 in HDR. Breakdown pressures were also similar for CO_2 stimulation in HDR and CO_2/PAA fluid system under identical injection flow rates. Finally, the well-known low viscosity of CO_2 phase prevents the efficient transport of proppants while the reacted CO_2/PAA fluid system is known to form a high viscosity binary fracturing fluid system with the potential to carry proppant in addition of being a fine fracturing fluid.

1. INTRODUCTION

Geothermal energy[1–4] is considered an alternative to fossil energy for that is attractive both because it is renewable and generates few CO_2 emissions. Low temperature, permeable (<150 °C) geothermal systems can be readily accessed employing similar drilling methods and technologies to tight oil recovery and without the need for stimulation operations due to the high permeability of the formation rock. However, these geothermal resources are limited to direct-use applications, such as district heating, greenhouses, fisheries, mineral recovery, and industrial process heating. Enhanced geothermal systems (EGS), on the other hand, are reservoirs often composed of highly impermeable igneous rock with access to temperatures between 150 and 450 °C and represent a very attractive renewable energy resource. After accessing the hot rock via drilling operations, hydraulic fracturing is recognized as an efficient way to increase the permeability of hot rock and, as a result, the heat exchange efficiency. However, unlike in low temperature settings (below 120 °C), oil and gas reservoirs, to fracture hot rock, operators need advanced stimulation fluids and tools that can withstand the high temperature environments. For example, gellants such as xanthan gum used to increase viscosity and enable proppant transport in tight oil and gas recovery cannot withstand temperatures above 120 °C. It is then critical to develop fracturing fluids that can efficiently fracture hot reservoirs without undergoing degradation of their chemical components. Another important economic and environmental problem during EGS stimulation operations is the heavy use of water. EGS fracturing operations require on average ten times the water[5,6] needed for tight oil stimulation operations. Therefore, research efforts have been also directed to develop alternative fluids that either require lower volumes of water or completely replace water while withstanding high temperature environments.

Towards this end, state-of-the-art waterless fluid technologies[7,8], including fluids such as N_2 and CO_2, have been explored, though at small scale. Propellants have also been investigated showing that the high-pressure pulses can generate fracture initiation and propagation, although concerns remain about their safe deployment and ability to propagate fractures very far beyond the well bore. Our group has recently developed CO_2-responsive fracturing fluids that undergo a volume expansion due to the crosslinking reactions between an aqueous polymer solution (polyallylamine 1wt%, PAA) and CO_2. These reactions and resulting volume expansion are triggered at high temperature. We postulated that this fracturing fluid, hereafter called StimuFrac™ or simply PAA, can mediate a reversible chemically-activated expansion and increase in viscosity[9–11] in confined environments. This volume expansion could provide a controllable increase of hydraulic pressure to aid in fracturing processes. Indeed, high pressure/temperature laboratory-scale experiments that simulated geothermal reservoir conditions at different depths (different confining P and T) demonstrated fracture creation on Coso geothermal samples and in non-porous fused silica samples with rock-like mechanical properties with the corresponding permeability enhancement.[11]

Nevertheless, questions remain around how we deploy/inject StimuFrac in an actual geothermal wellbore to take the most advantage of the CO_2-triggered volume expansion and rheo-reversible properties. In this work, we report on a series of fracturing experiments in larger (1/2-foot side) cubic rocks to evaluate StimuFrac (PAA aqueous solution) / CO_2 stimulation fluid against water, CO_2, and water/CO_2 fluids. The results, in terms of permeability enhancement, water volumes used, CO_2 volumes used, and net pressure required to initiate and propagate fractures in a surrogate rock (granite) are compared for all four fluid systems.

2. MATERIALS AND METHODS

2.1. Description of the hydraulic fracturing stimulation system

The schematic and different modules of the true-triaxial hydraulic fracturing system are shown in **Figure 1** and **Figure 2**. The true-triaxial hydraulic fracturing system consists of a rock sample placed into a confinement frame, together with four fluid-filled steel bladders called flatjacks. A set of wedges and shims fill the anulus between the frame and the sample so that each flatjack is fit snugly against the rock sample. When pressurized, each flatjack applies a stress to the lateral surfaces of the sample to simulate conditions in the deep subsurface. Efficiency tests were conducted to measure the relationship between the fluid pressure in the flatjack and the resulting stress in the sample. This empirical relationship was used to choose the fluid pressure that would produce the desired stress state within the rock. Throughout this paper we will refer to the applied stresses applied to the sample rather than the fluid pressure in the flatjacks. Fluid pressure is applied to the flatjacks by ISCO pumps. Fluid used is a hydraulic oil with boiling point well above that of the testing temperature so that the fluid in the flatjacks is not superheated. The entire loading frame and sample are outfitted with electrical heaters and thermocouples and wrapped in insulation to maintain temperature. Loading in the vertical direction is applied using a loading frame and set of stainless-steel load distribution plates. For reference the three directions are labeled as top-bottom (T-B), east-west (E-W), and north-south (N-S) according to their orientation in the laboratory. These are simply convenient labels and are not meant to represent the principal stress directions of any particular field site.

Fluid is then injected into a wellbore in the center of the sample so as to create a hydraulic fracture in the sample. Injection fluids will be composed of a mix of water, polymer (or surfactant), and CO_2. The hydraulic fracturing stimulation system is heated with four high temperature heaters wired in parallel (2" diameter, 1.5" width, 300 Watts, 120V AC). The heaters are plugged into an Extech PID controller using a type-J thermocouple attached to the outside of the fracturing system for feedback. A ground wire has been securely clamped to the fracturing system. The casing for fluids injection is shown in **Figure 3**. The casing is fixed in the well bore (Ø=5/16") by a pair of O-rings which helps for fluid pressurization during the fracturing test. The CO_2 is injected in a concentric line with 1/32" tubing diameter as shown in the cartoon on the left of **Figure 3** while water is injected in the outside large tubing with 1/4" tubing diameter.

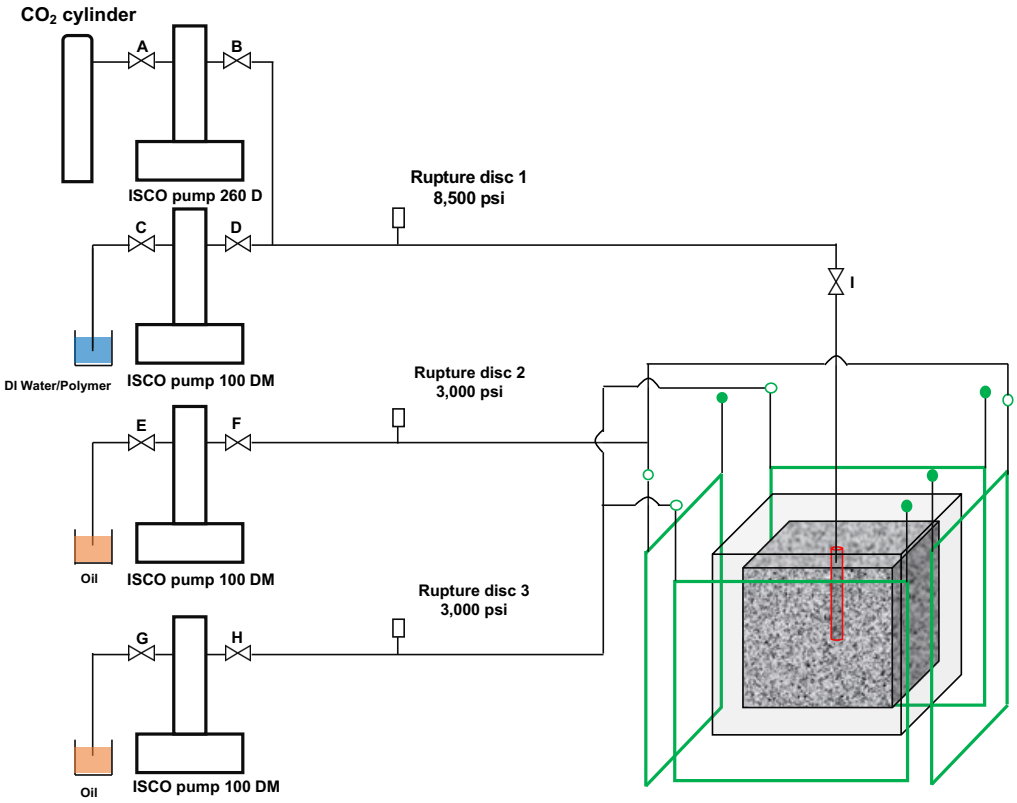

Figure 1 Diagram of hydraulic fracturing set-up

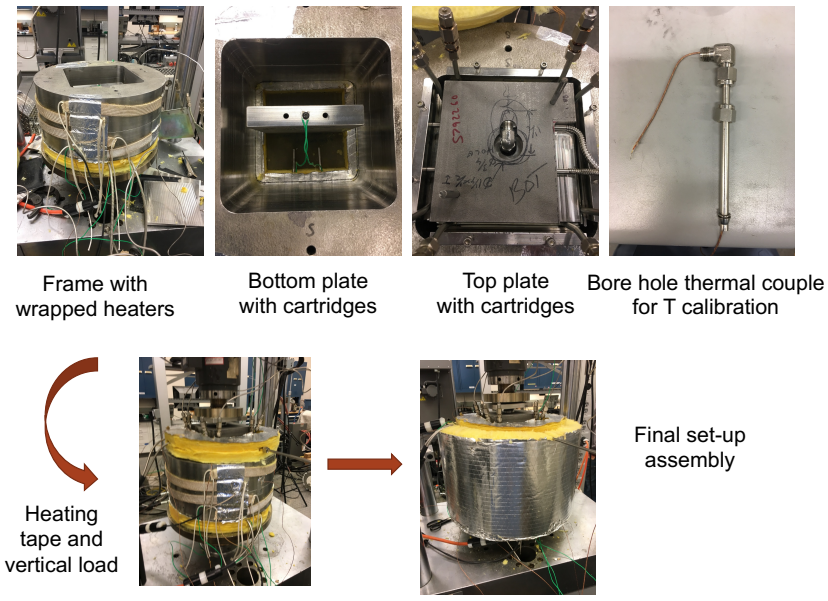

Figure 2 Different modules of hydraulic fracturing set-up

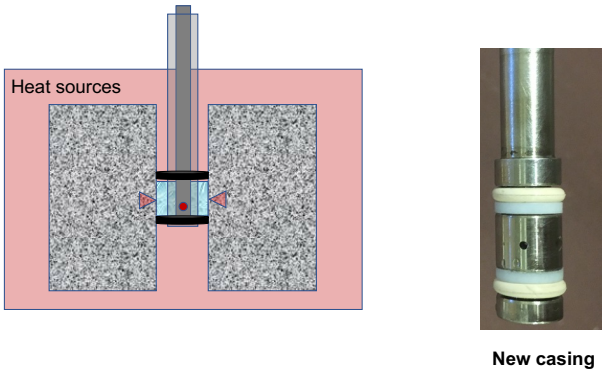

Figure 3 Casing and well bore design for hydraulic fracturing set up; Drawing not to scale

2.2. Fracturing procedure

A borehole is drilled longitudinally through each sample as shown in **Figure** 3. The sample is placed in the apparatus discussed in the previous section. The loading frame creates the principal stress difference that directs the fracture orientation as occurs in the field. The stress field used in this test is $\sigma_{T-B}/\sigma_{N-S}/\sigma_{W-E}$=7.58/9.65/9.65 MPa (1100/1400/1400 psi) which means the stress in the direction perpendicular to the top and bottom of the rock sample is the minimum principal stress and its value equals 7.58 MPa (1100 psi). The other two stresses are perpendicular to the south and north faces and to the east and west faces, respectively, and are equal to 9.65 MPa (1400psi). Control experiments were performed under identical temperature conditions. The results obtained for both control fluids (water and CO_2) will be used to compare all other injection approaches. The hydraulic fracturing tests include utilizing two fracturing fluids: water and CO_2 with different rock initial saturations. Four different stimulation tests are performed on half-foot cubic rock samples (Sierra White granite), as shown in **Figure 4,** either with constant pressure injection mode or constant flow rate mode. A notch in the horizontal (radial) direction was created (about 0.1mm deep) and the wellbore was polished to facilitate the introduction of the casing without damaging the O-rings that provide the zonal isolation.

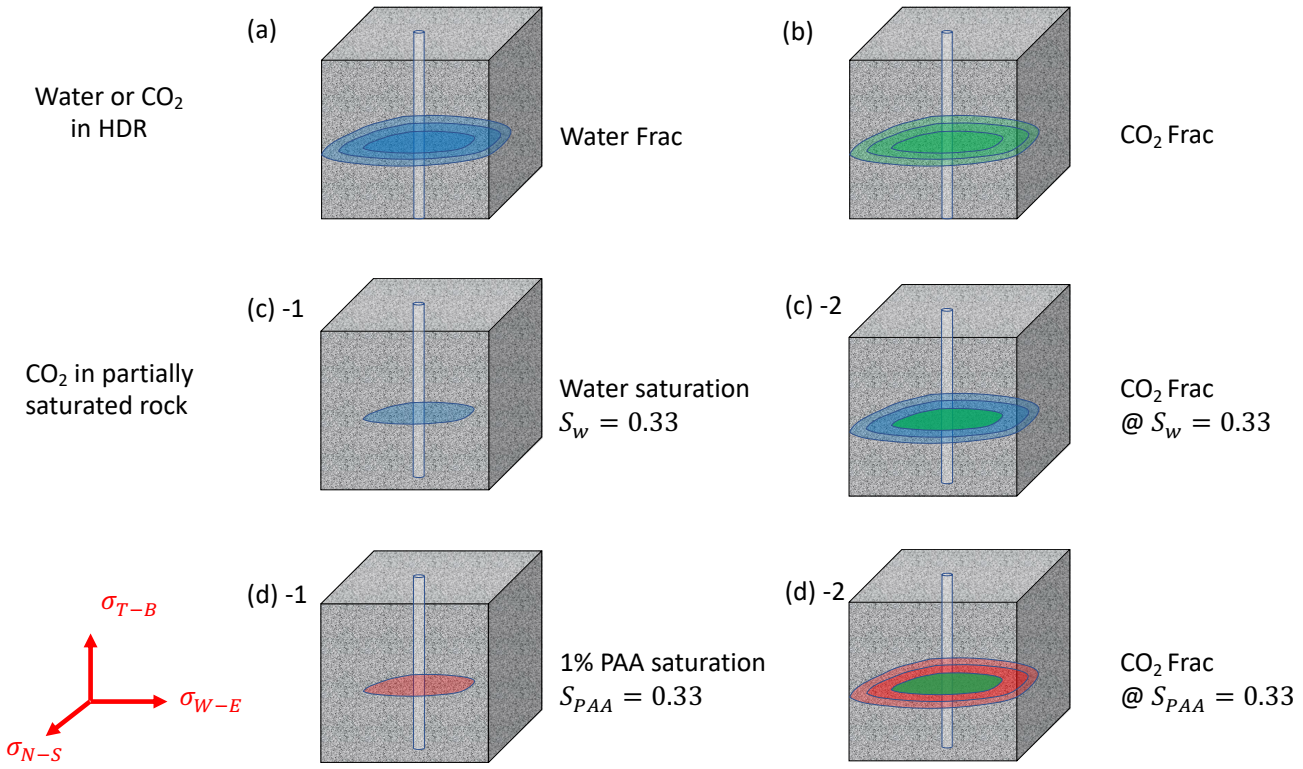

Figure 4 Four injection strategies for hydraulic fracturing including (a) water fracturing in hot dry rock (HDR); (b) CO_2 fracturing in HDR; (c) CO_2 fracturing with rock pre-saturated with water $\boldsymbol{S_w}$=0.33; (d) CO_2 fracturing with rock pre-saturated with aqueous PAA $\boldsymbol{S_{PAA}}$=0.33; Rock dimension=6" ×6"× 6"

Four stimulation strategies or stimulation fluids were used, each of which differ in the initial fluid saturation conditions they create in the sample, and/or in which fluid is used to drive the fracture. For each of the four strategies the fracture can be driven using either a constant-rate injection or using a series of constant-pressure steps. The following four paragraphs each describe one of the four strategies.

For the first stimulation strategy, referred to in **Figure 4(a)**, water was first injected in constant-pressure mode at 6.89MPa (1000 psi) which is higher than water/steam phase transition pressure 1.55 MPa (225 psi). After the flow rate due to leakoff reached nominally steady state, the water fracturing was initiated with constant flow rate mode or constant pressure mode until the rock fracture is estimated to have been driven to the edge of the sample. In the plots shown later in the paper, this strategy is labeled simply **H_2O**.

For the second strategy, referred to in **Figure 4(b)**, CO_2 is first injected in constant-pressure mode at 8.96 MPa(1300 psi) until the flow rate due to leakoff reached nominally steady-state. After that, the CO_2 fracturing is initiated with constant flow rate mode or constant pressure mode until the fracture is estimated to have been driven to the edge of the sample. In the plots shown later in the paper this strategy is labeled simply **CO_2**.

For the third strategy, CO_2 injection in water partially saturated porous matrix referred to in **Figure 4(c)**, water is injected into the wellbore in constant-pressure mode at 8.96 MPa(1300 psi) until a pre-defined volume of water has been injected. The volume of fluid was chosen to be equal to 1/3 of the estimated pore volume. The porosity was estimated to be 1%. This should result in an initial aqueous phase saturation equal to approximately 0.33. After this pre-saturation phase, CO_2 is injected in constant-pressure mode at 8.96 MPa (1300psi). After the flow rate due to leakoff reached nominally steady-state the sample (about 300 seconds) is then fracture with CO_2 in either constant pressure (pressure is hold for around 300 seconds at each pressure step) or constant flow-rate mode. In the plots shown later in the paper this strategy is referred to as **CO_2/H_2O**.

The fourth strategy, CO_2 injection in porous matrix partially saturated with an aqueous solution of PAA referred to in **Figure 4(d)**, is identical to strategy the CO_2/H_2O strategy except that instead of pre-saturating with water, a 1% PAA/water solution was used. In the plots shown later in the paper this strategy is referred to as **CO_2/PAA**.

2.3. Estimation of fracture conductivity, permeability and aperture

After the fracturing test but with the sample still under load and heated, the hydraulic conductivity of rock was measured via a series of injection tests using either oil (Dynalene HT oil) or water. Based on the stress field used in this study, the fracture will propagate on a

plane which is perpendicular to the direction of the minimum principal stress. The permeability or conductivity of fracture should be in between of the following two cases, $k_{low} < k_f < k_{high}$.

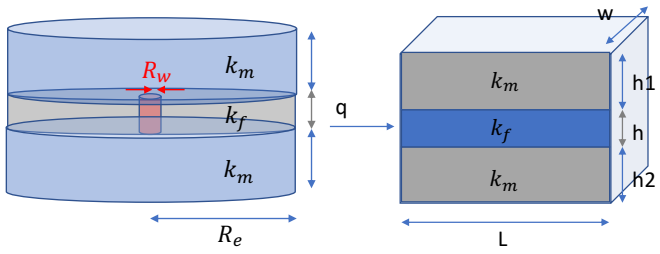

(a) (b)

Figure 5(a) Fracture completely generate a plane and it reach to the 4 surrounding surfaces, $\boldsymbol{k_{f,low}}$ (b) Fracture propagate to one of the four surfaces with a cuboid shape path, $\boldsymbol{k_{f,high}}$

For case 1, which is for single phase flow in radial direction as shown in **Figure 5(a)**, the volumetric flow rate as a function of radius of flow front is shown in Eq 1. The conductivity of the rock can be calculated based on Eq. 2.

$$\boldsymbol{Q = \frac{2\pi * k_{f,low} * h * (P_e - P_w)}{\mu * ln\frac{R_e}{R_w}}} \tag{1}$$

$$C_{f,low} = k_{f,low} \cdot h = \frac{Q * \mu * ln\frac{R_e}{R_w}}{2\pi * (P_e - P_w)} \tag{2}$$

Where Q is the volumetric flow rate; P_e is the pressure of the formation; P_w is the pressure of the wellbore; R_e is the radius of the formation; R_w is the radius of the wellbore; μ is the viscosity of fluids; $k_{f,low}$ is the lower limit of fracture permeability, h is the aperture of fracture.

For case 2, which is for 1-D single phase flow as shown in **Figure 5(b)**, the flow rate as a function of pressure gradient is shown in Eq. 3 and the conductivity of the fracture can be calculated based on Eq. 4.

$$q = \frac{Q}{w} = -\frac{k_{f,high} \cdot h \cdot \nabla p}{\mu} \tag{3}$$

$$C_{f,high} = k_{f,high} \cdot h = -\frac{Q\mu}{w\nabla p} = \frac{Q\mu L}{w\Delta p} \tag{4}$$

Where Q is the volumetric flow rate; w is the width of the fracture; ∇P is the pressure gradient across the rock; μ is the viscosity of fluids; $k_{f,high}$ is the upper limit of fracture permeability; h is the aperture of fracture.

The estimation of fracture permeability and aperture can be calculated based on cubic law. It is assumed after the fracture is formed; the fluid is flowing through a parallel plate. For Poiseuille flow in plane, the volumetric flow rate is a function of the aperture of the plate, which is known as cubic law as shown in Eq. 5 and Eq. 8. Based on Darcy's law for 1-D single phase flow as shown in Eq 6, the permeability and aperture of fracture could be calculated as shown in Eq.7 and Eq. 8. The permeability or conductivity is in between $k_{f,low}$ and $k_{f,high}$.

$$q = -\frac{h^3 \cdot \nabla p}{12\mu} \tag{5}$$

$$q = \frac{Q}{w} = -\frac{k_f \cdot h \cdot \nabla p}{\mu} \tag{6}$$

$$k_f = \frac{h^2}{12} \tag{7}$$

$$C_f = k_f \cdot h = \frac{h^3}{12} \tag{8}$$

Where Q is the volumetric flow rate; w is the width of the fracture; ∇P is the pressure gradient across the rock; μ is the viscosity of fluids; h is the aperture of fracture; k_f is the fracture permeability; C_f is the fracture conductivity.

3. RESULTS AND DISCUSSIONS

3.1. Stimulation with water: fracturing initiation, propagation, autogenous healing mechanisms

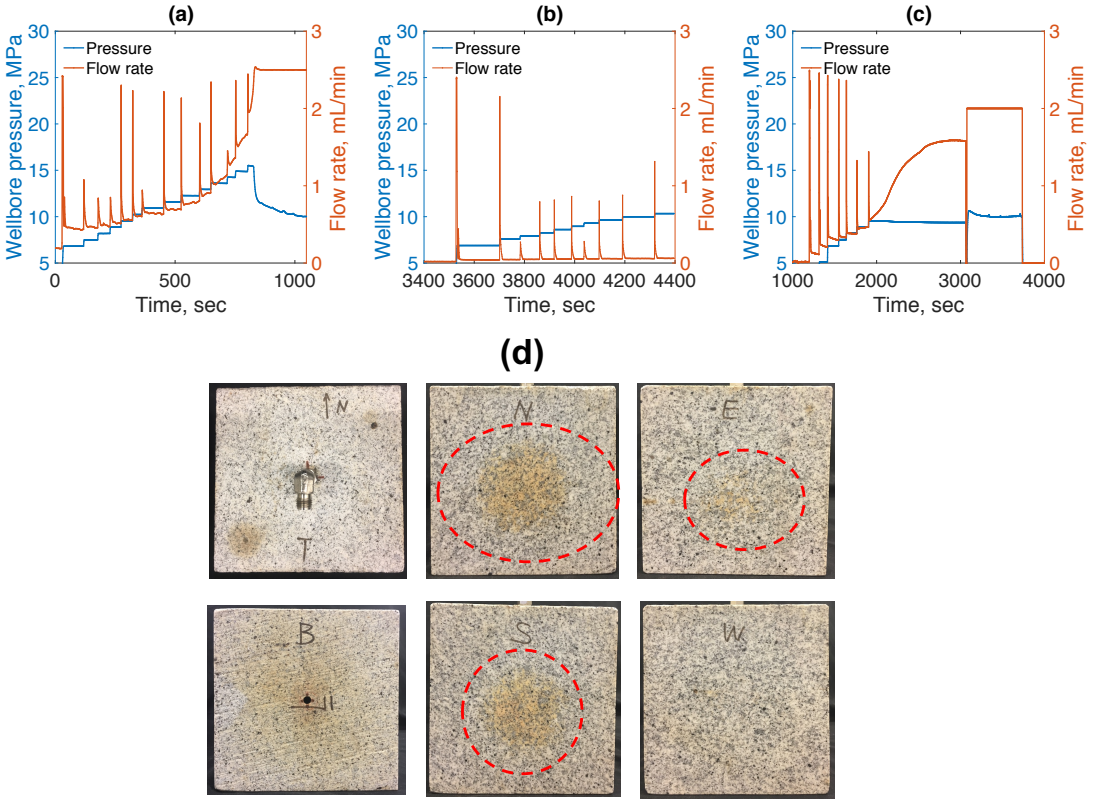

Figure 6 (a) Water fracture initiation, (b) fracture autogenous healing, (c) fracture's reopening, (d) photographs of the three fractured sides in the granite sample after reopening of the fracture.

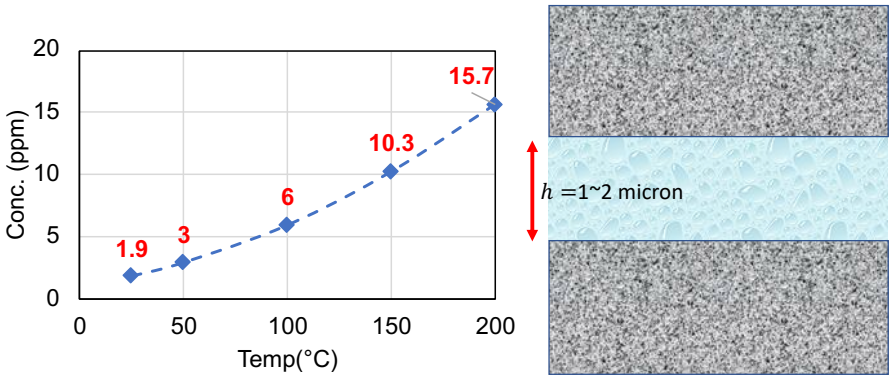

Figure 7. Computations of Si concentration in silica/water system at different temperatures; p=15.17 MPa (2200 psi)

A representative fracturing test conducted using the first strategy, i.e., water injection in hot dry rock (HDR) is shown in **Figure 6(a)**. The fracture initiation pressure is difficult to determine accurately from the pressure record. It appears to have occurred somewhere as low as 11.72 MPa (1700 psi), where there is clearly an increase in flow rate during the constant pressure hold, and certainly by 13.79 MPa (2000 psi), where there is an increase in rate during the pressure hold. The increase in the flow rate could be both, a result of fluid flowing out of the wellbore/pump and into the fracture (an increase in the system volume), and a result of increased leak off as new fracture surface area is exposed to the pressurized fluid. The flow rate increases during each pressure step until about 13.79 MPa (2250 psi) at which point the fracture begins to grow unstably right around 1220 seconds in **Figure 6(a)**. Following the sharp decline in pressure between 800 and 850 sec, the pressure declined more gradually, which would be interpreted as slow, leak off-dominated fracture growth until pumping is stopped at about 1450 sec. When the fracture grew unstably a volume of fluid that was originally stored elastically in the wellbore/pump is discharged into the fracture. After the system is cooled down to room temperature, the fracture is found to be healed and there is no breakthrough water observed from the rock surface. The healing process is confirmed by a subsequent injection experiment done at room temperature on the same sample as shown in **Figure 6(b)**, where at each pressure there is no obvious change of leak off flow rate of water. The healing rate for the fracture can be expressed as follows[12]:

$$\frac{dh}{dt} = \frac{Q \cdot C_p}{A_c \cdot \rho} \tag{9}$$

Where: h is the aperture of fracture, t is the time, C_p is the concentration of quartz in the effluent, ρ is the density of quartz. A_c is the contact area between two fracture surfaces; Q is the volumetric flow rate.

Under flowing conditions, dh/dt is reported as[12] 10^{-5}~10^{-7} μm/s in the temperature range of 80~150 ºC. PHEREEQC, which is a geochemical software available from the U.S. Geological Survey (USGS), was utilized for computing the Si concentration. Based on results of PHREEQC computations[13,14] as shown in **Figure 7**, it is likely that the injected water in the fracture at 200 ºC had a significant amount of dissolved silica. As the temperature falls over during the cooling down process this water could have become oversaturated with silica, causing the its precipitation and "healing" the fracture. In this experiment, after 70 h, the aperture of the rock would have been reduced by up to 2.5 μm based on equation 9. This estimated aperture reduction due to silica precipitation explain the lack of fracture conductivity since the fracture aperture generated by the hydraulic fracturing experiment as shown in **Figure 6 (a)** is estimated in 1.4~1.7 μm. After that, the rock is heated to 200 ºC, and the fracturing test using water with constant pressure mode is conducted again as shown **Figure 6 (c)**, which shows the fracture re-opens with a net pressure of about 10 MPa (1450 psi) demonstrating that the fracture had developed significant cohesion, presumably due to mineral precipitation during cool down. It is important to note that when switching to constant flow rate at about 3100 seconds, three pressure pulses were observed at 3300 seconds, 3500 seconds, and 3700 seconds, corresponding to the breakthrough of water in three different sides of the rock sample, as shown in Figure 6 (d). In order to inhibit self-healing of the hydraulic fracture, after the rock is fractured, an oil (Dynalene HT oil) slug is injected into the rock to inhibit the fracture autogenous healing in subsequent fracturing tests.

3.2. Stimulation with CO_2

Figure 8 shows the fracturing tests performed injecting CO_2 in HDR. The CO_2 fracturing was conducted at (a) constant P mode, (b) constant flow mode (4 mL/min), (c) constant flow mode (10 mL/min). The pressure for CO_2 was pressurized to 8.96MPa(1300psi) within pump before injection. For constant pressure mode fracturing as shown in **Figure 8(a)**, the pressure at each step change was hold for around 300 seconds until the rock get fractured ultimately. For fracturing using constant flow rate as shown in **Figure 8(b)** and **Figure 8(c),** CO_2 was pressurized to 8.96MPa (1300psi) first, then the constant flow rate (4 mL/min or 10 mL/min) of CO_2 was injected into the wellbore until the rock fractured.

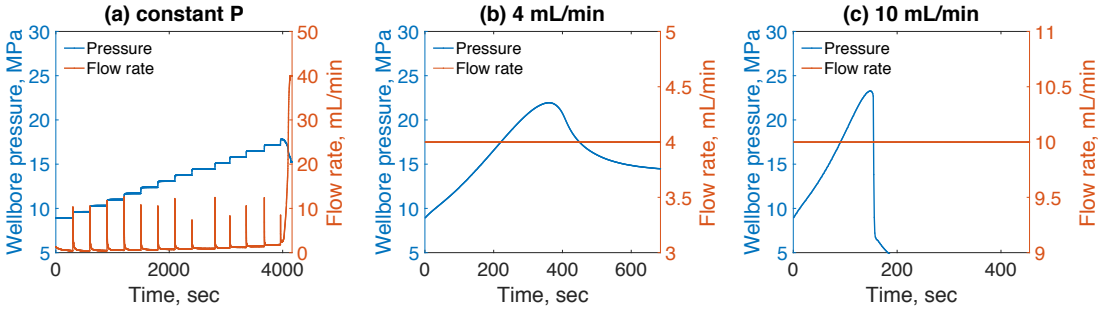

Figure 8 CO_2 fracturing at (a) constant P mode, (b) constant flow mode (4 mL/min), (c) constant flow mode (10 mL/min)

3.3. Stimulation with CO_2/H_2O

Figure 9(a) shows one of the fracturing tests performed injecting water at constant pressure to saturate about 1/3 of the total pore volume (TPV) followed by injection of CO_2 in discrete pressure increments. For constant pressure mode as shown in **Figure 9(a)**, the pressure at each step change was hold for around 300 seconds until the rock get fractured ultimately. For fracturing using constant flow rate as shown in **Figure 9 (b)** and **Figure 9 (c),** CO_2 was pressurized to 8.96MPa (1300psi) first, then the constant flow rate (2 & 3 mL/min or 10 mL/min) of CO_2 was injected into the wellbore after 1/3 of the TPV saturated with water. For the constant flow rate fracturing with 2 mL/min as shown in **Figure 9(b)**, the pressure gets stabilized after reaching to the steady state. The flow rate was increased to 3 mL/min afterwards, however, no rock breakdown was found. The pressure increases at first when flow rate increases to 3 mL/min, and then reduces to the pressure level when flow rate was equals to 2 mL/min. The pressure fluctuation during 3 mL/min may be caused by the water saturation changes due to drainage at high fractional flow of wetting phase.

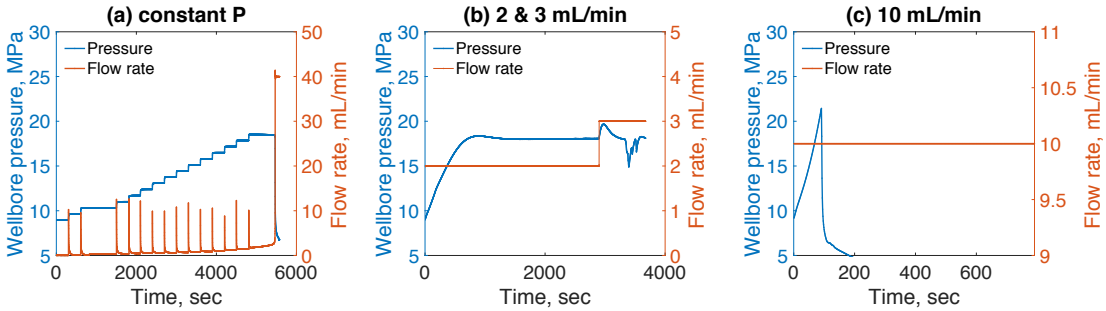

Figure 9 CO_2/H_2O fracturing at (a) constant P mode, (b) constant flow mode (2~3 mL/min), (c) constant flow mode (10 mL/min)

3.4. Stimulation with CO_2/PAA

Similar to the above described injection of CO_2 in a rock matrix partially saturated with water (1/3 of TPV), CO_2 was injected in granite with 1/3 of the TPV saturated with a 1 wt% aqueous solution of PAA. **Figure 10(a)** shows one of the fracturing tests performed injecting a PAA solution at constant pressure to saturate about 1/3 of the TPV followed by injection of CO_2 in discrete pressure increments. For constant pressure mode as shown in **Figure 10(a)**, the pressure at each step change was hold for around 300 seconds until the rock get fractured ultimately. For fracturing using constant flow rate as shown in **Figure 10 (b)** and **Figure 10 (c),** CO_2 was pressurized to 8.96MPa(1300psi) first, then the constant flow rate (2 mL/min or 10 mL/min) of CO_2 was injected into the wellbore with 1/3 of the TPV saturated with a 1 wt% aqueous solution of PAA. Unlike the case where the rock is saturated with water in **Figure 9** (b), CO_2 can fracture the rock when the rock is 2 mL/min.

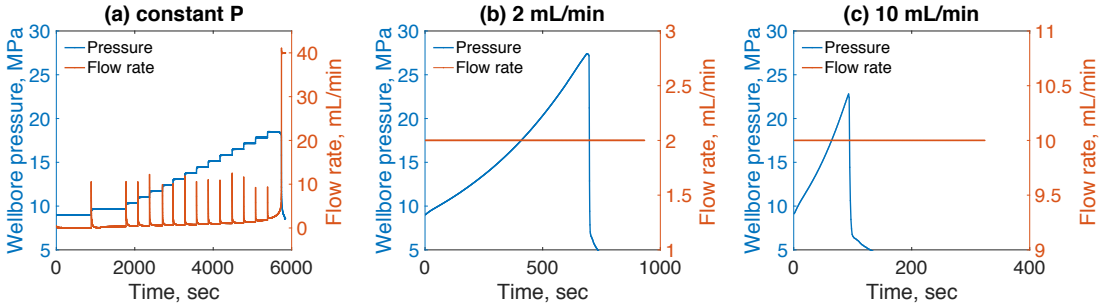

Figure 10 CO_2/PAA fracturing at (a) constant P mode, (b) constant flow mode (2 mL/min), (c) constant flow mode (10 mL/min)

3.5. Diagram of conductivity and breakdown pressure (Pb)/pressurization rate

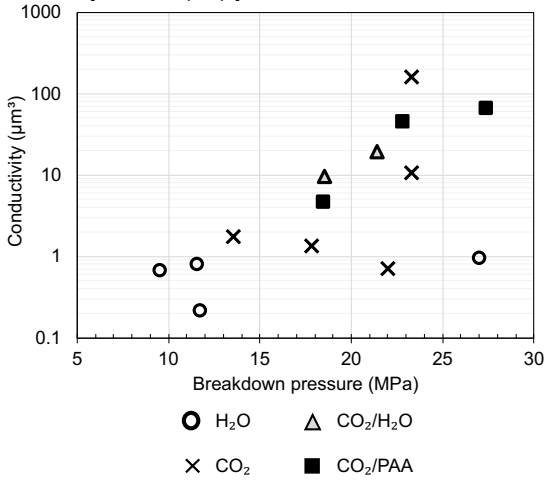

Figure 11 Diagram of conductivity and breakdown pressure of fracturing results (see Section 2.2 for detailed explanations); note that for each injection strategy some data points the injection rate and mode (constant pressure vs. constant rate) differ, which explains some of the scatter in the data; see **Figure 12** for a similar plots with groupings by injection mode

Figure 11 shows the diagram of conductivity versus the breakdown pressure for different fluids assisted fracturing processes. All the tests were conducted at high temperature (200 ºC) conditions. **Table 1** shows a summary of the constant flow rate and constant pressure fracturing tests. The breakdown pressure, fracture conductivity, permeability and aperture, water (or 1% PAA) and CO_2 mass consumption are also included in **Table 1**.

The circle symbols in **Figure 11** represent the first stimulation strategy, water fracturing in HDR. The breakdown pressure ranged from 9.65 MPa (1400 psi) to 11.72 MPa (1700 psi), with a fracture conductivity of less than 1 μm^3 independently of injection regime, i.e. constant pressure increments or constant flow rates. Furthermore, even with an injection flow rate as high as 25 mL/min and a breakdown pressure of 26.89 MPa (3900 psi) the fracture hydraulic conductivity was still below 1 μm^3. The second stimulation strategy, i.e., CO_2 fracturing in HDR (cross symbols in **Figure 11**) can generate fracture with a wide range of conductivity values. For two tests using constant pressure mode, low conductivity fractures are generated by discrete increments in CO_2 pressure. When injecting CO_2 in HDR using constant flow mode the conductivity is also low for low/intermediate flow rates but increases significantly (10.8~23.1 μm^3 and 160~341 μm^3) at high flow rates though with fracture conductivity values that differ by an order of magnitude. CO_2/H_2O stimulation strategy (triangle symbols in **Figure 11**), i.e. injecting water at constant pressure to saturate 0.33 of TPV followed by injection of CO_2 in discrete pressure increments or at constant flow rate showed relatively high fracture conductivity than water in HDR or CO_2 in HDR when comparing constant pressure injection regimes. However, and similarly to CO_2 injection in HDR, fracturing efficiency was negligible at low injection rates and only good at high injection rates (10 mL/min) with conductivity values in the 19.6~41.8 μm^3 range. The fourth stimulation strategy, CO_2/PAA (square symbols in **Figure 11**), with constant pressure injection mode fractured granite at similar

breakdown pressures than CO_2/H_2O but obtaining fractures with slightly lower conductivity than when fracturing with CO_2/H_2O. However, in constant flow rate mode, CO_2/PAA attained two of the largest conductivity values (44.7~95.0 μm^3 and 65.7~139.5 μm^3) which were not influenced by injection flow rate. Still, the breakdown pressures were higher than CO_2/H_2O stimulation strategy and similar or higher than CO_2 in HDR. It is also important to note that CO_2/PAA stimulation strategy consistently generated highly conductive fractures independently of injection mode (constant pressure or constant flow rate) and pressurization rate.

Table 1 Summary of fracturing results with different stimulation strategies/fluids with constant pressure or flow rate injection modes

Test	Mode/Rate	Strategy	P_b	C_f	K_f	h	m_{H_2O} / m_{PAA}	m_{CO_2}
	(mL/min)		(MPa)	(μm^3)	(μm^2)	(μm)	(g)	(g)
1	C_P	H_2O	*11.72	*0.2~0.4	*0.2~0.3	*1.4~1.7	8.3	0
2	C_P	H_2O	9.53	0.7~1.5	0.3~0.6	2.0~2.6	1.2	0
3	C_P	CO_2	13.52	1.8~3.8	0.7~1.1	2.8~3.6	0	43.7
4	C_P	CO_2	17.80	1.3~2.8	0.5~0.9	2.5~3.2	0	49.6
5	C_P	CO_2/H_2O	18.53	9.7~20.5	2.0~3.3	4.9~6.3	11.3	42.4
6	C_P	CO_2/PAA	18.48	4.7~10.0	1.22~2.0	3.8~4.9	11.3	55.9
7	$C_Q = 2$	H_2O	11.55	0.8~1.7	0.4~0.6	2.1~2.7	0.9	0
8	$C_Q = 25$	H_2O	27.01	1.0~2.1	0.4~0.7	2.3~2.9	0.6	0
9	$C_Q = 4$	CO_2	21.95	0.7~1.5	0.4~0.6	2.0~2.6	0	9.7~14.5
10	$C_Q = 10$	CO_2	23.70	160.6~341.1	12.9~21.3	12.4~16.0	0	7.8~12.8
11	$C_Q = 10$	CO_2	23.28	10.8~23.1	2.2~3.6	5.0~6.5	0	4.0~8.3
12	$C_Q = 2\ or\ 3$	CO_2/H_2O	N/A	No frac	No frac	No frac	11.3	4.3~21.1
13	$C_Q = 10$	CO_2/H_2O	21.44	19.7~41.8	3.2~5.3	6.2~7.9	11.3	0~2.5
14	$C_Q = 2$	CO_2/PAA	27.40	65.7~139.5	7.1~11.8	9.2~11.9	11.3	1.1~4.9
15	$C_Q = 10$	CO_2/PAA	22.81	44.7~95.0	5.5~9.1	8.1~10.5	11.3	0~2.3

**Note: C_P means constant pressure; C_Q means constant flow rate

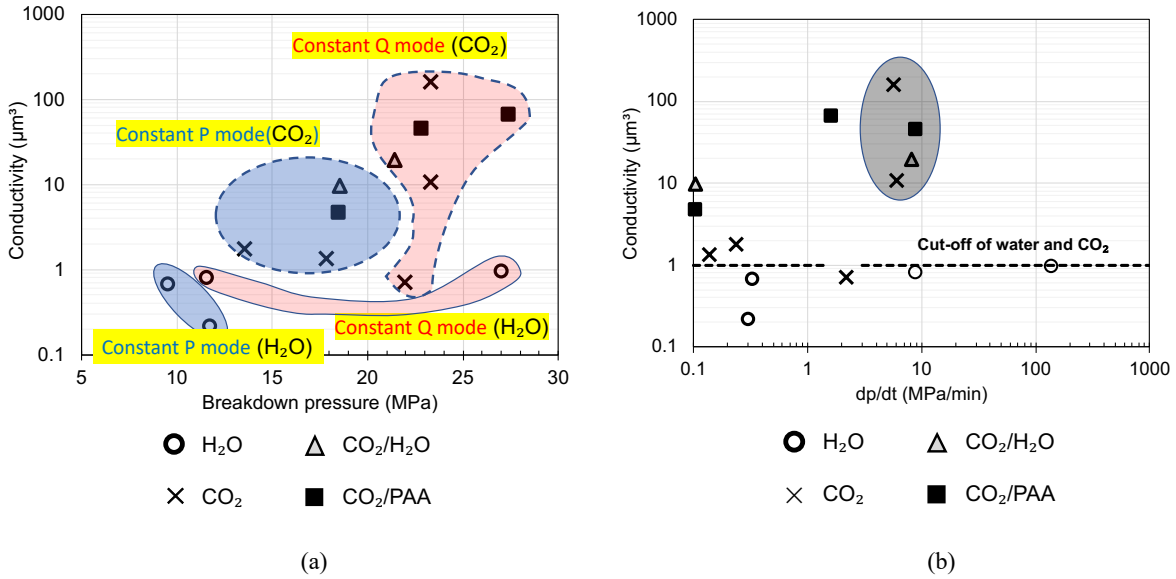

(a) (b)

Figure 12 (a) conductivity versus breakdown pressure with different injection mode; (b) conductivity of fracture generated as a function of pressurization rate of fluids injected

As shown in **Table 1**, for the CO_2/H_2O stimulation strategy, when the flow rate of injected CO_2 equals to 2mL/min or 3 mL/min, the rock does not fracture because the leakoff from the wellbore exceeds this flow rate. Similarly, when injecting CO_2 in HDR, low/intermediate flow rates generate low fracture conductivity (entry 9 in Table 1). Constant pressure injection mode generally consumes more CO_2 than constant flow rate mode due to the time spent during the pressure holds at each step. This can be noted by comparing entries 3 and 4 versus entries 9-11 (stimulation strategy CO_2 in HDR) or by comparing entry 5 against entries 12 and 13 and entry 6 with entries 14 and 15.

Figure 12(a) is complementary to **Figure 11** since the fracturing results are divided into two regimes based on the injection mode, i.e. constant pressure mode or constant flow rate mode. High conductivity values of fracture are obtained when the breakdown pressure is high. For all stimulation strategies or fluids constant flow rate mode (once it overcomes the leak off all the way to Pb), is more effective in generating higher conductivity fractures than constant pressure mode. This is likely due to the high transient flow rate to the fracture following breakdown, which is enhanced by the higher compressibility of CO_2 compared to water. The constant pressure injection modes result in much more stable fracture propagation and lower transient flow rates since the fracture is more leakoff-dominated in this mode. The transient flow rate following breakdown, though it also occurs in the field, can be viewed as an artifact of the reduced scale testing since in the field it would influence only the very near wellbore region. The majority of the fracture in a field setting would be expected to be created in more of a stable propagation regime, which is more closely represented by the constant pressure injection tests in the laboratory. As stated earlier, the CO_2/PAA stimulation strategy resulted in slightly higher conductivity than the CO_2/H_2O strategy for the constant flow rate mode, and slightly lower for the constant pressure mode.

Figure 12(b) shows the effect of pressurization rate of fracturing fluids on the fracture conductivity. Pressurization rate is calculated based on the fluid pressure increase divided by time before rock break down. In general, for all stimulation strategies, the higher the pressurization rate, the higher is the fracture conductivity. The exception are all the tests conducted with the H_2O in HDR strategy, where the conductivity of fracture generated is less than 1μm^3 for both constant flow rate and constant pressure tests. For the second stimulation strategy, CO_2 in HDR, the first rapid fracturing with 10 mL/min generates the highest conductivity (160.6~341.1 μm^3). However, when performing a second identical CO_2 in HDR with 10 mL/min the fracture generated is (10.8~23.1 μm^3) even through the breakdown pressure for both tests is the same. The same applies to stimulation strategies CO_2/H_2O and CO_2/PAA. As shown in the grey colored regime in **Figure 12** (b), when the pressurization rate is around 5~10 MPa/min, the conductivity of the fracture is large. As stated earlier, CO_2/PAA stimulation strategy consistently generated highly conductive fractures independently of pressurization rate as can be seen in entry 14 of **Table 1**. The reason for this will be discussed next.

3.6. Well bore history of fracturing fluids with constant pressure injection mode

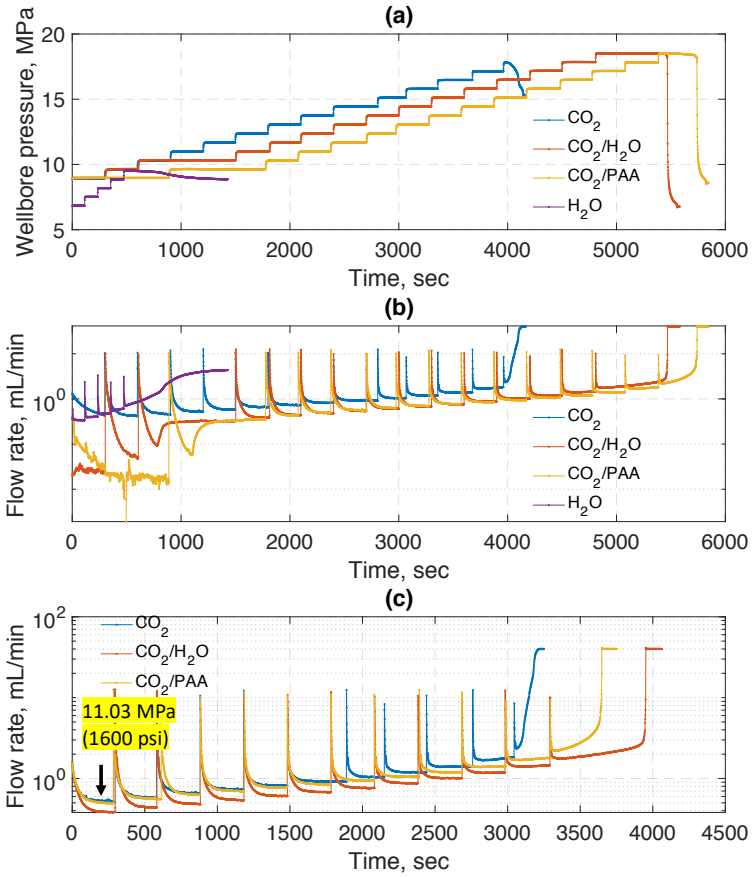

Figure 13 (a) Well bore pressure history of all four stimulation strategies in constant-pressure mode (b) pump flow rate history of all four stimulation strategies in constant-pressure mode; (c) flow rate history with pressure =11.03 MPa (1600 psi) as starting point of three stimulation strategies, CO_2 in HDR, CO_2/H_2O, and CO_2/PAA at constant pressure. All tests were conducted at 200°C.

Figure 13(a) and **Figure 13(b)** shows the wellbore pressure and flow rate history of injected fracturing fluids for all the stimulation experiments performed at constant pressure mode. It is observed that tests with the H_2O in HDR stimulation strategy have much lower breakdown pressure than all other stimulation strategies. For the CO_2 in HDR stimulation strategy, shown in the blue curve in **Figure 13(a)**, the breakdown pressure is 17.80 Mpa (2582 psi). While for CO_2/H_2O and CO_2/PAA stimulation strategies, the breakdown pressure is between 18.48 MPa (2681 psi) and 18.53 MPa (2687 psi), which is about 0.7MPa (100 psi) higher than that of the CO_2 in HDR strategy.

As the fluid pressure increases in discrete steps, the flow rate increases. According to Darcy's law for single phase flow, the flow rate is proportional to the pressure gradient applied. This is the reason why the flow rate increases almost linearly with pressure before fracturing takes place. Once the fracture is initiated, the conductivity of the whole rock system is dynamically increasing which leads to an increasing leak off rate of the fracturing fluids.

In order to compare the results, the flow rate data of three stimulation strategies involving CO_2, i.e. CO_2 in HDR, CO_2/H_2O, and CO_2/PAA is plotted in **Figure 13**(c). The starting point of the flow rate is when pressure switches to 11.03 MPa (1600 psi). The results show that at each pressure stage, the leak off rate of CO_2 is different. The stimulation strategy CO_2 in HDR resulted in the highest leak off rate among the three tests. This is explained by the fact that in this stimulation experiment there is no water in the rock matrix, thus there is no relative permeability issue which impedes the leak off of CO_2 into the porous matrix. For the CO_2/PAA and CO_2/H_2O stimulation strategy tests with constant pressure steps, the leak off rate at each pressure stage is different from each other under same pressure gradient conditions. After wellbore pressure of the rock approaches to the breakdown pressure, the CO_2 flow rate increases as a function of time.

For constant pressure CO_2 in HDR stimulation test, the flow rate reaches the maximum pump delivery rate and in the shortest time. On the other hand, in the constant pressure CO_2/H_2O stimulation test the flow rate reaches the maximum pump delivery rate with the longest time while for constant pressure CO_2/PAA stimulation test, the flow rate reaches the maximum pump delivery rate at an intermediate time. This shows then that the leak off rate of the CO_2/H_2O stimulation test is lower than the CO_2/PAA test. The opposite effect is observed on experiments at constant flow rate (refer to Section 3.7) though we don't currently have an explanation for this. As shown in **Table 1**, the conductivity for the constant pressure CO_2 in HDR stimulation test is the lowest(1.34~2.84 μm^3), with highest conductivity for constant pressure CO_2/H_2O (9.7~20.5 μm^3) and followed very closely by the conductivity for constant pressure CO_2/PAA stimulation (4.7~10.0 μm^3).

3.7. Well bore history of fracturing fluids with constant flow rate injection mode

Figure 14 shows wellbore pressure history with all four stimulation strategies/fluids performed in constant flow rate mode. **Figure 14(a)** shows that using water in HDR as the stimulation strategy generates fractures at significantly higher breakdown pressures at higher flow rates. However, the transient flow rate is low and, as shown in **Table 1**, with generation of very low conductivity fractures. For comparative purposes, water in HDR stimulation strategy is shown in **Figure 14(a-d)**. **Figure 14(a)** also shows results with the second stimulation strategy, CO_2 in HDR. Fracturing test injecting at 4mL/min in CO_2 in HDR shows that the rock is fractured with a slow fracture propagation process (dark blue plot) and at a relatively high breakdown pressure, while the final fracture conductivity is the lowest among all the successful fracturing tests. The conductivity of the fracture is as low as 0.7~1.5 μm^3 as shown in **Table 1**. However, when the flow rate of CO_2 in HDR is increased to 10mL/min, the rock can be fractured much faster [orange and red plots in **Figure 14(a)**], and a much larger conductivity of fracture can be created. Two fracturing tests at 10 ml/min constant flow rate were performed using the CO_2 in HDR stimulation strategy, and the two results show a good match of all the data points before the rock breaks down as shown in **Figure 14**(b). For the first of these tests, the breakdown pressure is 23.27 MPa (3375 psi) while for the second test it is 23.28 MPa (3376psi). However, once the fracture initiates, the two tests show a notably different behavior for CO_2 transport in the rock with fracture propagation. From the pressure response, the two curves deviate from each other once the pressure of the wellbore is around 6.21 MPa (900 psi) (which is just below the minimum principal stress of 7.58 MPa (1100 psi)). This suggests that above this point, i.e., when the fracture is generated and open, there is a positive net pressure and the two fractures have similar hydraulic properties. However, once the fractures are closed (at a negative net pressure), the two fractures behave differently. The first stimulation test with CO_2 in HDR shows a much sharper pressure decline curve below 6.21 MPa (900 psi) which indicates a significantly larger fracture compared to the second stimulation test since the pump flow rate of CO_2 is identical in the two tests (10 mL/min). The conductivity measured for the largest fracture is around 160.6~341.1 μm^3 (first stimulation test with CO_2 in HDR at 10 mL/min) while for the second test performed under identical conditions the fracture conductivity is around 10.8~23.1 μm^3. The reason of why these two-fracturing tests shows nearly identical breakdown pressure but very different conductivity is still unclear. One of the possible hypotheses could be associated to differences in rock heterogeneity or even minute natural fractures which could exists in the rock matrix systems which interferes in the fracture propagation process.

Figure 14(c) shows results for CO_2/H_2O and CO_2/PAA stimulation strategies/fluids (the two solid curves are the well bore pressure as a function of time for these two tests. These tests were carried out with a CO_2 flow rate of 2-3 mL/min in rock partially saturated with water or PAA (1/3 of TPV). For the fracturing test with CO_2/H_2O stimulation fluid, the sample does not fracture the rock due to the leak off rate accommodating the entire injected flow rate of CO_2. The pressure reaches a plateau at a constant flow rate of 2 mL/min. However, for a fracturing test performed with CO_2/PAA stimulation fluid, there is a pressure curve separation from that of the CO_2/H_2O stimulation test at ~250 seconds and pressure ~15.17 MPa (2200 psi) as shown in **Figure 14**(c). The curve separation could be caused by 1) in-situ crosslinking reaction between CO_2 and PAA, 2) volume expansion induced saturation increase of aqueous phase. As shown in Eq 11, the increased water saturation could cause a reduction of relative permeability for the supercritical CO_2 phase. Therefore, when the superficial velocity of the supercritical CO_2 phase is constant, the pressure gradient will increase according to Darcy's law as shown in Eq 10.

$$\mu_g = -\frac{k_{rock} * k_{rg}}{u_g} * \nabla \mathrm{P} \tag{10}$$

Where k_{rock} is permeability of rock; k_{rg} is the relative permeability of gas; ∇P is the pressure gradient across the rock; u_g is the superficial velocity.

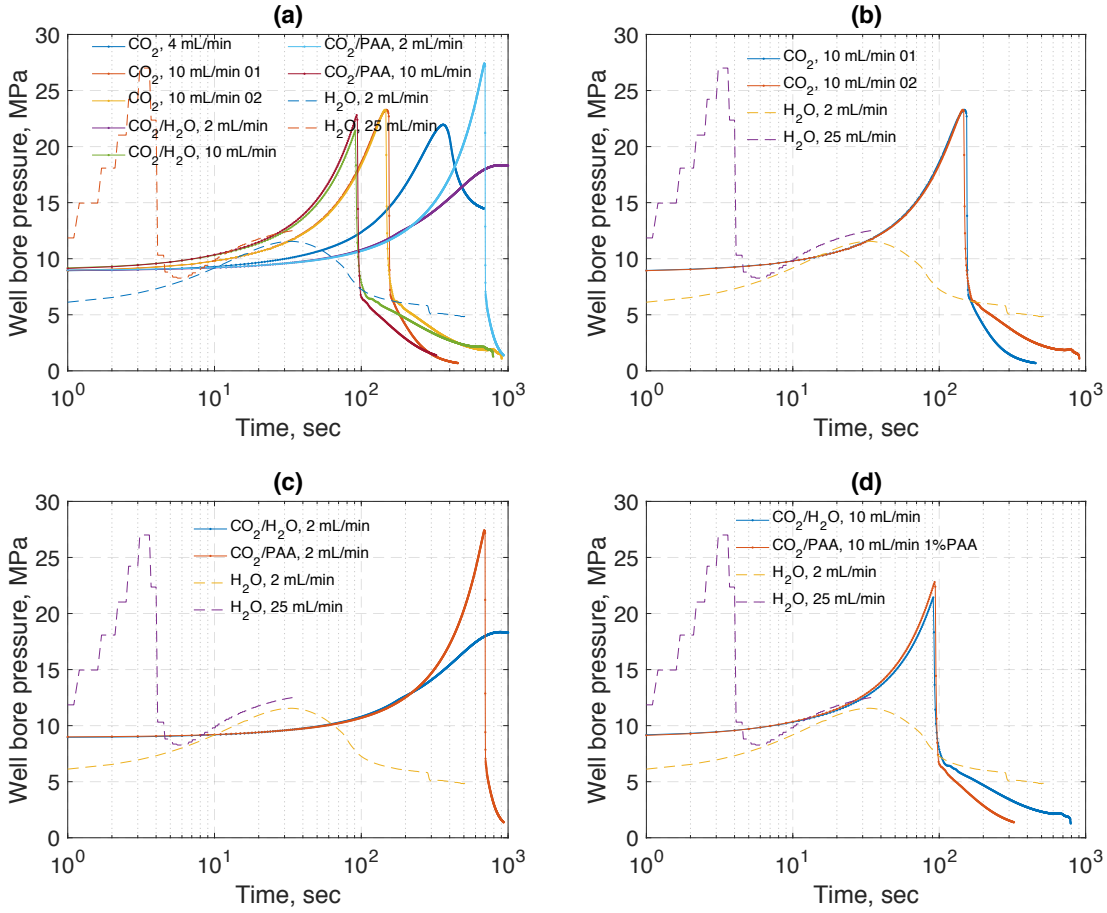

Figure 14 (a) Well bore pressure history of all four stimulation strategies in constant flow rate mode; (b) two CO_2 in HDR stimulation tests with constant flow rate Cq=10mL/min; (c) a CO_2/H_2O and CO_2/PAA stimulation test with constant flow rate Cq=2 mL/min; (d) a CO_2/H_2O and CO_2/PAA stimulation test with constant flow rate Cq=10 mL/min. Plots of water in HDR stimulation tests with Cq=2 mL/min and Cq=25 mL/min injection rates are shown in all four Figures as reference (dashed lines). All stimulation tests were conducted at 200°C.

For a CO_2/H_2O two-phase saturated system, the relative permeability of the gas phase[15] based on Corey's model is expressed as shown in Eq.11.

$$k_{rg} = k_{rg}^{0} * \left(\frac{1-S_w-S_{wc}}{1-S_{grw}-S_{wc}}\right)^{n_g} \tag{11}$$

Where k_{rg}^{0} is the end point relative permeability of gas; S_w is the water saturation; S_g is the gas saturation; S_{wc} is the connate water saturation; S_{grw} is the residual gas saturation to water; n_g is the exponent coefficient of gas in Corey's relative permeability model.

For high flow rate stimulation tests, CO_2/H_2O (10 mL/min) and CO_2/PAA (10 mL/min), the results show that in the presence of PAA the increase of pressure is sharper than that in the presence of water [**Figure 14(d)**]. Furthermore, this could also be caused by the saturation increase of aqueous phase induced by PAA/CO_2 in-situ crosslinking reaction in the porous media. Similar to the plots shown in **Figure 14(c)**, stimulation test with CO_2/PAA (10 mL/min) shows a much sharper pressure decline curve below 6.21 MPa (900 psi) than the stimulation test with CO_2/H_2O (10 mL/min) which indicates a significantly larger fracture attained by PAA/CO_2 stimulation fluid. Indeed, the fracture conductivity obtained by stimulating with CO_2/PAA stimulation fluid is higher than that of CO_2/H_2O stimulation fluid independently of injection rates (entries 12-15 in **Table 1**), making PAA/CO_2 stimulation fluid a very good alternative for fracturing in EGS.

3.8. Flow rate into fracture during constant flow rate fracturing tests by different stimulation fluids

The transient flow rate into fracture[16] can be calculated using Eq. 12.

$$Q_{frac} = Q_{pump} - 1/C * dp/dt \quad (12)$$

Where Q_{frac} is the flow rate into fracture; Q_{pump} is the flow rate delivered from the pump; C is the compressibility of the overall fracturing fluid system; dp/dt is the derivative of pressure to time.

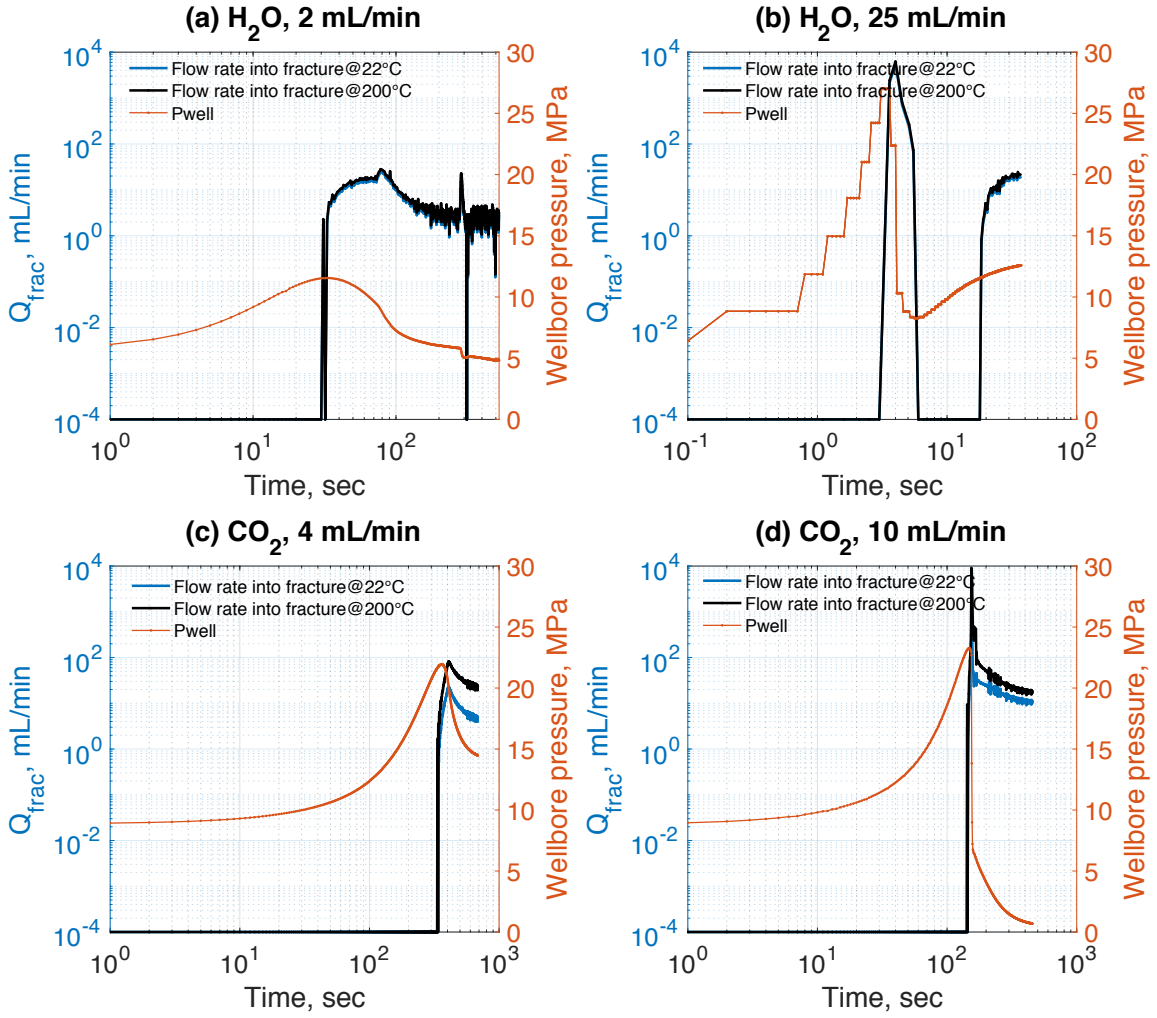

Figure 15 (a)Cq2_ H_2O fracturing; (b) Cq25_ H_2O fracturing; (c)Cq4_ CO_2 fracturing; (d) Cq10_ CO_2 fracturing; all the test is conducted @200°C. **Zero or negative flow rate to fracture is set to 10^{-4} mL/min, which allows plots with loglog scale.

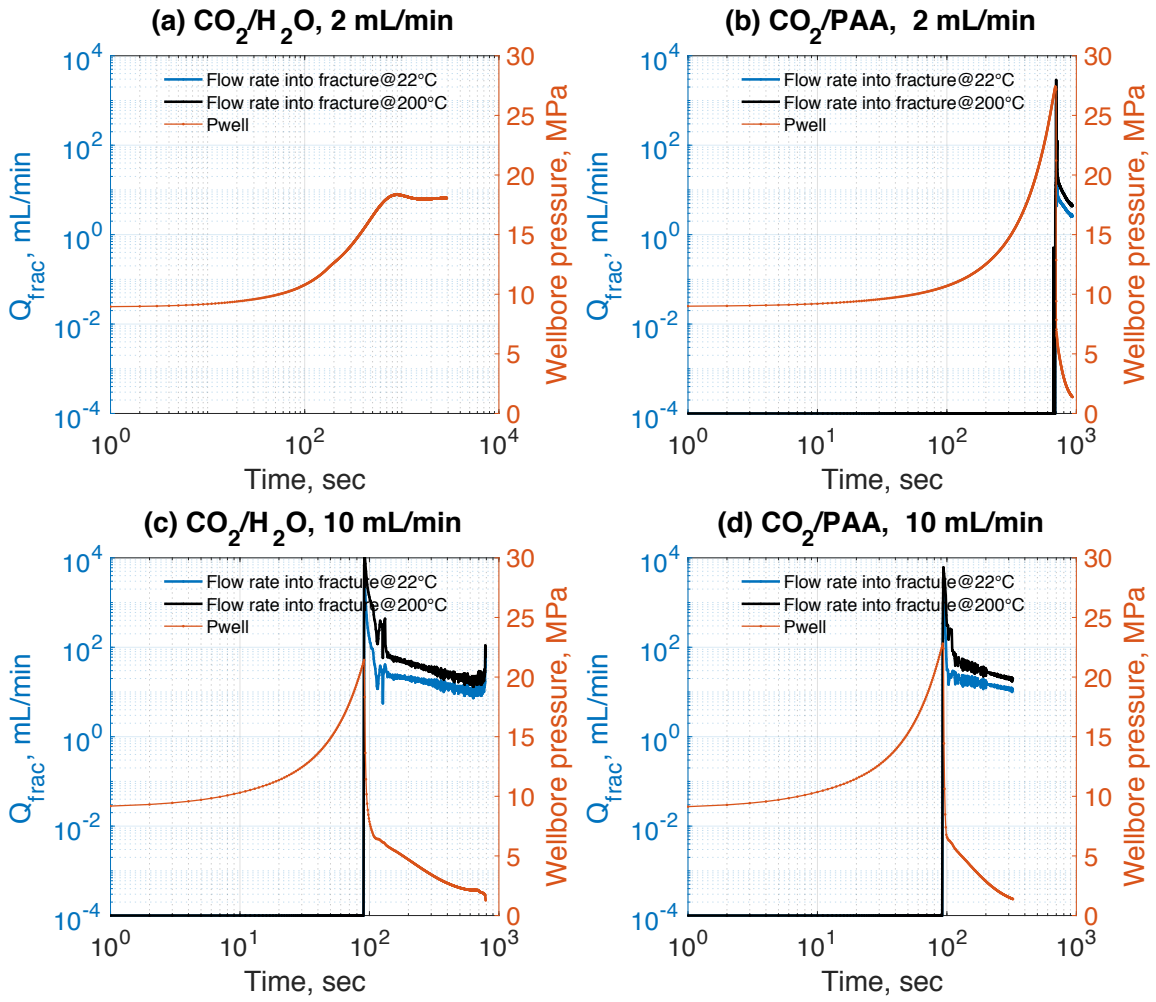

Figure 16 (a) Cq2_ CO_2 +0.33 PV Water; (b)Cq10_ CO_2 +0.33 PV Water; (c)Cq2_ CO_2 +0.33 PV-PAA fracturing; (d) Cq10_ CO_2 +0.33 PV-PAA fracturing; all the tests are conducted @200°C. **Zero or negative flow rate to fracture is set to 10^{-4} mL/min, which allows plots with loglog scale.

The results of flow to fracture for different stimulation tests are shown in **Figure 15** for water in HDR and CO_2 in HDR and in **Figure 16** for stimulation strategies CO_2/H_2O and CO_2/PAA. For all fracturing tests involving CO_2 except the case of CO_2 in HDR stimulation strategy with 4 mL/min injection flow rates and CO_2/H_2O stimulation strategy with 2-3 mL/min, the maximum transient flow rate is in the range of 0.5×10^4~1×10^4 mL/min, while it is only ~10^2 mL/min for the CO_2 in HDR (4 mL/min) test and 0 for CO_2/H_2O (2-3 mL/min) as no fracture was generated. This can be interpreted as a slower, more stable and leakoff-dominated fracturing process when CO_2 is injected at 4 mL/min in HDR. No fracture was attained when CO_2 is injected at 2-3 mL/min in partially water-saturated (0.33 of TPV) rock. The conductivity of the fracture obtained by fracturing with CO_2 injected in HDR at 4 mL/min is also the lowest, 0.7~1.5 μm^3, among all the stimulation tests using CO_2. While for other constant flow rate fracturing strategies that use CO_2, either in HDR (stimulation strategy 2) or in a binary fluid system (CO_2/H_2O at 10 mL/min and CO_2/PAA) the conductivity values are all above 10 μm^3. High conductivity fractures are hypothesized to be caused by the high transient fluid rate to fracture rather than the fluid properties. In other words, the slow leakoff-dominated process seems to generate a less conductive fracture than the more rapid propagation process.

In order to investigative whether the high transient fluid rate can generates fractures with high conductivity for all the stimulation fluids (water- or CO_2-based), a fracturing test using the water in HDR stimulation strategy with high flow rate (25 mL/min) was conducted as shown in **Figure 15(b)**. **Figure 15(a)** shows the fracturing results using 2 mL/min water injection, the conductivity of fracture is around 0.8-1.7 μm^3 and the maximum transient flow rate to fracture is in the range of 10~10^2 mL/min. Conversely, for the stimulation test using 25 mL/min of water in HDR, the maximum transient flow rate into fracture is approaching to 10^4 mL/min which is similar to that of most of the CO_2-based (single fluid or binary fluids) fracturing tests. However, the conductivity of the fracture for 25 mL/min of water in HDR is only 1.0~2.1 μm^3. This indicates that a high transient flow rate into fracture is not the only element required to generate fractures with high conductivity. The properties of the fluid itself also play a key role in the fracture creation and propagation.

4. SUMMARY

A high-temperature true-triaxial system was used to evaluate four stimulation strategies/fluids in granite at 200 °C. These are 1) water in HDR, 2) CO_2 in HDR, 3) CO_2 in the presence of water partially saturated rock (1/3 of TPV), and 4) CO_2 in the presence of rock partially saturated with an aqueous solution of 1wt% PAA (1/3 of TPV). A specially designed wellbore casing allows the injection of fracturing fluids with different injection modes (constant pressure increments or constant flow rate regimes). For stimulation strategy 1, water in HDR, the supersaturated silica in the water phase could cause the fracture to heal completely as a function of time when the rock temperature is decreased after stimulation and in the absence of flow.

The breakdown pressure was higher for tests with all stimulation strategies that used CO_2, particularly when using constant flow rate injection modes, as compared to fracturing with only water. The discrepancy between these results and those in the literature[7,17] is not yet understood, but it may be cause by the difference of temperature (room temperature vs 200 °C) and rock type (shale vs. granite).

Results show that for water in HDR stimulation strategy, the conductivity is generally less than 1 μm^3 (radial flow) even with high flow rate (25 mL/min) water fracturing. For CO_2-based stimulation fluids, i.e. CO_2 in HDR, CO_2/H_2O, and CO_2/PAA, the fracture conductivity is generally larger than that of water independently of injection mode, constant pressure steps or constant flow rate. These finding are consistent with other results published in the literature, for both shale and granite at room temperature.[7]

Pressurization rate of CO_2 is a key factor for generating fractures with high conductivity. Rapid pressurization rate (>6.89 MPa/min (1000 psi/min)) of CO_2 is beneficial for generating fractures with higher conductivity (>10 μm^3). However, when the pressurization rate of CO_2 is lower than 0.69MPa/min (100 psi/min), the hydraulic conductivity (1~10 μm^3) of the fracture is slightly higher than that of water (<1 μm^3). This is also contradictory to other results published in the literature, which attributed the enhanced conductivity of CO_2-generated fractures to additional stimulation by the additional leakoff volume associated with CO_2 as compared to water. In our study the higher injection rates, which would produce less leakoff overall, resulted in more conductive fractures.

Injection of water or PAA to partially saturate the rock previous to CO_2 injection (stimulation strategies CO_2/H_2O and CO_2/PAA) is beneficial to reduce the leak-off rate of CO_2 fracturing test. The leak-off rate of CO_2 can be significantly reduced using PAA for constant flow rate fracturing process, and this can be explained by the fact that the CO_2-triggered crosslinking reaction of PAA and associated volume explanation can cause in-situ increase of aqueous phase saturation, thus decrease the relative permeability of CO_2 phase. As a result, it is easier for CO_2 to build up pressure and create larger fractures as compared to CO_2/H_2O stimulation fluid. In addition, the transient flow rate of fracturing fluids especially for the CO_2-based stimulation fluids (CO_2 in HDR, CO_2/H_2O, and CO_2/PAA) can affect the ultimate conductivity of the created fracture. For CO_2-based stimulation processes, fractures with large conductivity can be formed if the transient flow rate to fracture is in the order of 10^4 mL/min.

It was found that CO_2 as a fracturing fluid injected in hot dry rock (HDR) attain the highest fracture conductivity though only when injected at very high flow rates. This performance is followed very closely by the CO_2/PAA fracturing fluid system that generates fractures with, on average, similarly high conductivity values though independently of injection flow rate. Breakdown pressures were also similar for CO_2 stimulation in HDR and CO_2/PAA fluid system under identical injection flow rates. CO_2/PAA fluid system requires nearly 1/6 of the mass of CO_2 required when stimulating with CO_2 in HDR (0-2.3g vs 4-12.8 g) but a corresponding mass of PAA equivalent to 0.11g (5% of that of CO_2) is also required. Finally, the well-known low viscosity of CO_2 phase prevents the efficient transport of proppants while the reacted CO_2/PAA fluid system is known to form a high viscosity binary fracturing fluid system with the potential to carry proppant in addition to be a fine fracturing fluid.

NOMENCLATURE

C_p	Concentration of quartz in the effluent
ρ	The density of quartz
A_c	The contact area between two fracture surfaces
Q	The volumetric flow rate
P_e	Pressure of the formation
P_w	Pressure of the wellbore
R_e	Radius of the formation
R_w	Radius of the wellbore
μ	Viscosity of fluids
$k_{f,low}$	Lower limit of fracture permeability
$k_{f,high}$	Upper limit of fracture permeability
k_{rock}	Permeability of rock
∇P	Pressure gradient across the rock
k_{rg}	Relative permeability of gas
k_{rg}^0	End point relative permeability of gas
S_w	Water saturation
S_g	Gas saturation

S_{wc} Connate water saturation

S_{grw} Residual gas saturation to water

n_g Exponent coefficient of gas in Corey's model

Q_{frac} The flow rate into fracture

Q_{pump} Flow rate delivered from the pump

C Compressibility of the overall fracturing fluid system

dp/dt Derivative of pressure to time.

REFERENCES

(1) Lund, J. W.; Freeston, D. H. World-Wide Direct Uses of Geothermal Energy 2000. *Geothermics* **2001**, *30* (1), 29–68. https://doi.org/10.1016/S0375-6505(00)00044-4.

(2) Lund, J. W.; Freeston, D. H.; Boyd, T. L. Direct Application of Geothermal Energy: 2005 Worldwide Review. *Geothermics* **2005**, *34* (6), 691–727. https://doi.org/10.1016/j.geothermics.2005.09.003.

(3) Lund, J. W.; Freeston, D. H.; Boyd, T. L. Direct Utilization of Geothermal Energy 2010 Worldwide Review. *Geothermics* **2011**, *40* (3), 159–180. https://doi.org/10.1016/j.geothermics.2011.07.004.

(4) Lund, J. W.; Boyd, T. L. Direct Utilization of Geothermal Energy 2015 Worldwide Review. *Geothermics* **2016**, *60*, 66–93. https://doi.org/10.1016/j.geothermics.2015.11.004.

(5) Chabora, E.; Zemach, E.; Spielman, P.; Drakos, P.; Hickman, S.; Lutz, S.; Boyle, K.; Falconer, A.; Robertson-Tait, A.; Davatzes, N. C. Hydraulic Stimulation of Well 27-15, Desert Peak Geothermal Field, Nevada, USA. In *Proceedings of thirty-seventh workshop on geothermal reservoir engineering, Stanford University, Stanford*; 2012; Vol. 30.

(6) Bradford, J.; Ohren, M.; Osborn, W. L.; McLennan, J.; Moore, J.; Podgorney, R. Thermal Stimulation and Injectivity Testing at Raft River, ID EGS Site. In *Proceedings of 39th Workshop on Geothermal Reservoir Engineering, Stanford, CA, USA*; 2014.

(7) Song, X.; Guo, Y.; Zhang, J.; Sun, N.; Shen, G.; Chang, X.; Yu, W.; Tang, Z.; Chen, W.; Wei, W.; et al. Fracturing with Carbon Dioxide: From Microscopic Mechanism to Reservoir Application. *Joule* **2019**, *3* (8), 1913–1926. https://doi.org/10.1016/j.joule.2019.05.004.

(8) Isaka, B. L. A.; Ranjith, P. G.; Rathnaweera, T. D.; Wanniarachchi, W. A. M.; Kumari, W. G. P.; Haque, A. Testing the Frackability of Granite Using Supercritical Carbon Dioxide: Insights into Geothermal Energy Systems. *Journal of CO2 Utilization* **2019**, *34*, 180–197. https://doi.org/10.1016/j.jcou.2019.06.009.

(9) Shao, H.; Kabilan, S.; Stephens, S.; Suresh, N.; Beck, A. N.; Varga, T.; Martin, P. F.; Kuprat, A.; Jung, H. B.; Um, W.; et al. Environmentally Friendly, Rheoreversible, Hydraulic-Fracturing Fluids for Enhanced Geothermal Systems. *Geothermics* **2015**, *58*, 22–31. https://doi.org/10.1016/j.geothermics.2015.07.010.

(10) B. Jung, H.; C. Carroll, K.; Kabilan, S.; J. Heldebrant, D.; Hoyt, D.; Zhong, L.; Varga, T.; Stephens, S.; Adams, L.; Bonneville, A.; et al. Stimuli-Responsive/Rheoreversible Hydraulic Fracturing Fluids as a Greener Alternative to Support Geothermal and Fossil Energy Production. *Green Chemistry* **2015**, *17* (5), 2799–2812. https://doi.org/10.1039/C4GC01917B.

(11) Fernandez, C. A.; Gupta, V.; Dai, G. L.; Kuprat, A. P.; Bonneville, A.; Appriou, D.; Horner, J. A.; Martin, P. F.; Burghardt, J. A. Insights into a Greener Stimuli-Responsive Fracturing Fluid for Geothermal Energy Recovery. *ACS Sustainable Chem. Eng.* **2019**, *7* (24), 19660–19668. https://doi.org/10.1021/acssuschemeng.9b04802.

(12) Polak, A.; Elsworth, D.; Yasuhara, H.; Grader, A. S.; Halleck, P. M. Permeability Reduction of a Natural Fracture under Net Dissolution by Hydrothermal Fluids. *Geophysical Research Letters* **2003**, *30* (20). https://doi.org/10.1029/2003GL017575.

(13) Parkhurst, D. L.; Appelo, C. A. J. User's Guide to PHREEQC (Version 2): A Computer Program for Speciation, Batch-Reaction, One-Dimensional Transport, and Inverse Geochemical Calculations. *Water-resources investigations report* **1999**, *99* (4259), 312.

(14) Parkhurst, D. L.; Appelo, C. A. J. *Description of Input and Examples for PHREEQC Version 3: A Computer Program for Speciation, Batch-Reaction, One-Dimensional Transport, and Inverse Geochemical Calculations*; US Geological Survey, 2013.

(15) Jian, G.; Zhang, L.; Da, C.; Puerto, M.; Johnston, K. P.; Biswal, S. L.; Hirasaki, G. J. Evaluating the Transport Behavior of CO2 Foam in the Presence of Crude Oil under High-Temperature and High-Salinity Conditions for Carbonate Reservoirs. *Energy Fuels* **2019**, *33* (7), 6038–6047. https://doi.org/10.1021/acs.energyfuels.9b00667.

(16) de Pater, C. J.; Cleary, M. P.; Quinn, T. S.; Barr, D. T.; Johnson, D. E.; Weijers, L. Experimental Verification of Dimensional Analysis for Hydraulic Fracturing. *SPE Production & Facilities* **1994**, *9* (04), 230–238. https://doi.org/10.2118/24994-PA.

(17) Ishida, T.; Aoyagi, K.; Niwa, T.; Chen, Y.; Murata, S.; Chen, Q.; Nakayama, Y. Acoustic Emission Monitoring of Hydraulic Fracturing Laboratory Experiment with Supercritical and Liquid CO2. *Geophysical Research Letters* **2012**, *39* (16). https://doi.org/10.1029/2012GL052788.